

High-order accurate difference schemes for the Hodgkin-Huxley equations

David Amsallem and Jan Nordström

Linköping University Post Print



N.B.: When citing this work, cite the original article.

Original Publication:

David Amsallem and Jan Nordström, High-order accurate difference schemes for the Hodgkin-Huxley equations, 2013, Journal of Computational Physics, (252), 573-590.

<http://dx.doi.org/10.1016/j.jcp.2013.06.035>

Copyright: Elsevier

<http://www.elsevier.com/>

Postprint available at: Linköping University Electronic Press

<http://urn.kb.se/resolve?urn=urn:nbn:se:liu:diva-96367>

High-order accurate difference schemes for the Hodgkin-Huxley equations

David Amsalle^a, Jan Nordström^b

^a*Department of Aeronautics and Astronautics, Durand Building, Room 028, 496 Lomita Mall. Stanford University, Stanford, 94305-4035, USA*

^b*Department of Mathematics, Linköping University, SE-581 83 Linköping, Sweden*

Abstract

A novel approach for simulating potential propagation in neuronal branches with high accuracy is developed. The method relies on high-order accurate difference schemes using the Summation-By-Parts operators with weak boundary and interface conditions applied to the Hodgkin-Huxley equations. This work is the first demonstrating high accuracy for that equation. Several boundary conditions are considered including the non-standard one accounting for the soma presence, which is characterized by its own partial differential equation. Well-posedness for the continuous problem as well as stability of the discrete approximation is proved for all the boundary conditions. Gains in terms of CPU times are observed when high-order operators are used, demonstrating the advantage of the high-order schemes for simulating potential propagation in large neuronal trees.

Key words: High-order accuracy; Hodgkin-Huxley; Neuronal networks; Stability; Summation-by-parts; Well-posedness

1. Introduction

Understanding the integration of synaptic input by a neuron and the propagation of the signal to its own output synapses is of high importance in neurosciences. Numerical simulation of such a phenomena has become an option since Hodgkin and Huxley developed their model in 1952 [1]. The Hodgkin-Huxley equations are a set of coupled partial and ordinary differential equations. The first one is the cable equation that describes the distribution and evolution of the intracellular potential. The other equations are related to the evolution of gating variables describing ion channels dynamics inside a neuron, which is typically constituted of dendritic branches, a soma, an axon and synapses. Appropriate boundary conditions can be associated with branch ends, junctions and the soma. The soma boundary condition is non-standard since it consists of a linear relation between time and space derivatives of the solution and the solution itself.

Subsequently, Rall developed methods for solving the potential propagation in passive neuronal trees where branches satisfying the “3/2” law are connected to the soma [2]. In the subsequent literature, the Hodgkin-Huxley equations were typically approximated using multi-compartmental models where each unknown corresponds to the value of the potential or gating variable inside a small compartment. Current conservation is then enforced, resulting in spatially second-order schemes such as in [3] where Hines simulated the potential propagation in a neuronal tree without soma. That scheme was subsequently used for predictions of potential propagation in dendritic trees with soma [4, 5].

A method for time integration of the coupled system formed by the cable and gating variables equations was proposed by Hines in [3] using a second-order accurate staggered Crank-Nicolson method. A first-order in time backward Euler monolithic scheme for the coupled Hodgkin-Huxley equations of a single branch with Neumann boundary conditions was then proposed in [6] together with a convergence proof. In [7], the

Email addresses: amsalle@stanford.edu (David Amsalle), jan.nordstrom@liu.se (Jan Nordström)
URL: stanford.edu/~amsalle (David Amsalle)

authors propose a first-order in time forward Euler scheme for the Hodgkin-Huxley equations with Dirichlet boundary conditions, as well as a convergence proof under a CFL condition.

In the present work, high-order accurate difference schemes based on Summation-By-Parts (SBP) operators with the weak Simultaneous Approximation Term (SAT) procedure [8, 9, 10, 11, 12, 13, 14, 15, 16, 17, 18] are applied to the Hodgkin-Huxley equations and their associated boundary conditions. Rigorous convergence properties are demonstrated for several types of boundary conditions, including the non-standard soma boundary condition. The ability to apply high order schemes for the solution of the Hodgkin Huxley equations is essential since it results in a lower computational cost for the large systems that arise when neurons with large dendritic trees are considered. It will be demonstrated that the SBP-SAT technique provides a modular approach that is particularly effective for coupling of branches in a dendritic tree. Indeed, the SBP-SAT method offers a very effective way to enforce potential continuity and current conservation at the junction between those branches.

This paper is organized as follows: in Section 2, the continuous set of partial differential equations and associated boundary conditions are presented and their strong well-posedness is demonstrated using energy estimates for two essential cases: (1) the case of an axon connected to the soma and (2) the case of a dendritic tree. In Section 3, discretization of each of the aforementioned problems is carried out and the associated penalty coefficients are chosen so that semi-discrete energy estimates hold. This results in identical estimates as in the continuous case and strong stability of the semi-discrete problem. In Section 4, the order of convergence associated with each of the two aforementioned problems is investigated using the method of manufactured solutions. Applications of the new proposed approach to large neuronal systems are reported in Section 5. Conclusions are drawn in Section 6.

2. The continuous problem

2.1. Equations

The Hodgkin-Huxley equations [1] are a set of coupled partial and ordinary differential equations expressed in terms of the (1) intracellular potential $u(x, t)$ and (2) gating variables $m(x, t)$, $h(x, t)$ and $n(x, t)$ describing ion channels dynamics. The computational domain is in this section $x \in [0, L]$.

The equation for the potential u is based on the cable equation [19] and can be written as

$$u_t = \frac{\mu}{a(x)}(a(x)^2 u_x)_x - \frac{1}{C_m}g(m(x, t), h(x, t), n(x, t))u + \frac{1}{C_m}f(m(x, t), h(x, t), n(x, t), x, t), \quad (x, t) \in [0, L] \times [0, T]. \quad (1)$$

In (1), $a(x)$ is the radius of the neuron at the location x , C_m the specific membrane capacitance and

$$\mu = \frac{1}{2C_m R_i} > 0,$$

where R_i denotes the axial resistivity. The conductance $g(m, h, n)$ of the cable in terms of the gating variables is

$$g(m, h, n) = g_1 m^3 h + g_2 n^4 + g_3, \quad (2)$$

where $g_i > 0$, $i = 1, 2, 3$. The expression for $f(m, h, n, x, t)$ is given by

$$f(m, h, n, x, t) = g_1 E_1 m^3 h + g_2 E_2 n^4 + g_3 E_3 - I(x, t), \quad (3)$$

where E_i , $i = 1, 2, 3$ are equilibrium potentials. $I(x, t)$ is an input current at location x that originates either from artificial current injection or synaptic input from another neuronal cell.

The equations describing the evolution of the gating variables are

$$\begin{aligned} m_t(x, t) &= \alpha_m(u(x, t))(1 - m(x, t)) - \beta_m(u(x, t))m(x, t), \\ h_t(x, t) &= \alpha_h(u(x, t))(1 - h(x, t)) - \beta_h(u(x, t))h(x, t), \\ n_t(x, t) &= \alpha_n(u(x, t))(1 - n(x, t)) - \beta_n(u(x, t))n(x, t). \end{aligned} \quad (4)$$



Figure 1 Outer normal vectors to a branch

where $(x, t) \in [0, L] \times [0, T]$. Expressions for $\alpha_m, \alpha_h, \alpha_n, \beta_m, \beta_h$ and β_n are provided in Appendix A.

One can prove the following property based on the equations associated with the gating variables.

Proposition 1. Let $x \in [0, L]$. If $0 \leq m(x, 0) \leq 1$ and if $m(x, t)$ is \mathcal{C}^0 in time, then $0 \leq m(x, t) \leq 1 \forall t \in [0, T]$.

Proof: see Appendix B.

The same property also applies for h and n . As a result, the function g can be bounded as follows

$$0 < g_3 \leq g(m, n, h) = g_1 m^3 h + g_2 n^4 + g_3 \leq \sum_{i=1}^3 g_i. \quad (5)$$

The bound (5) will be useful when well-posedness of the initial boundary value problems is studied in Section 2.6.

Several types of boundary conditions can be associated with the cable equations [19].

2.2. Voltage clamp boundary conditions

The simplest boundary condition associated with Eq. (1) is the prescribed potential condition at $x_b = 0$ or $x_b = L$:

$$u(x_b, t) = u_0(t). \quad (6)$$

This corresponds to controlling the potential at the extreme end of the cable. This is often performed by electrophysiologists using a voltage clamp constituted of a current generator with two electrodes.

2.3. Sealed end boundary conditions

Another possible boundary condition for Eq. (1) is the sealed end boundary condition at $x_b \in \{0, L\}$:

$$\nabla u(x_b, t) \cdot n(x_b) = 0, \quad (7)$$

where $n(x_b)$ is the outer normal vector to $[0, L]$ at the end point x_b of the cable, as depicted in Figure 1. $\nabla u(x_b, t) \cdot n(x_b)$ corresponds, up to a constant factor, to the current that exits the domain $[0, L]$ at x_b . Hence, enforcing the sealed end boundary conditions is equivalent to prescribing that there is no current exiting the neuron at x_b . This boundary condition holds when an extremity of a cable is not attached to any other cable or the soma.

Remark. Although the field u only depends on one space variable, in the remainder of the paper, the notation $\nabla u(x_b, t) \cdot n(x_b)$ is used in place of $-u_x(x_b, t)$ when x_b is a left boundary (that is $n(x_b) = -1$) and in place of $u_x(x_b, t)$ when x_b is a right boundary ($n(x_b) = 1$).

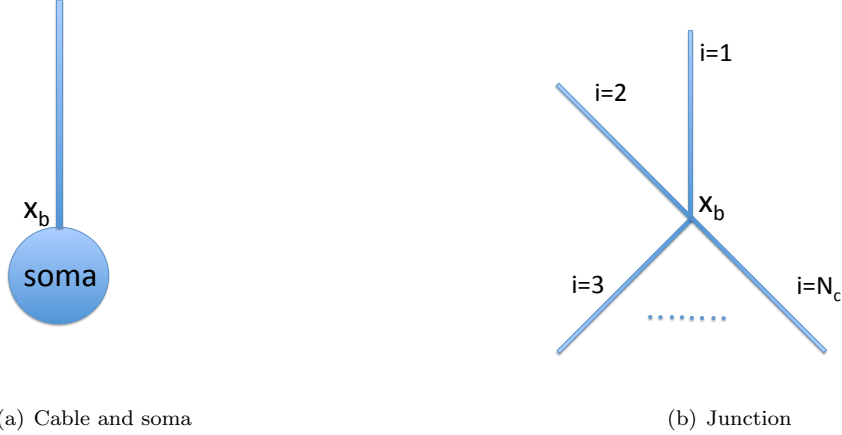


Figure 2 Two configurations for a neuronal network

2.4. Soma boundary conditions

When a soma is located at an extremity x_b of a cable, a boundary condition describing the current conservation in the soma applies [19]. This configuration is graphically depicted in Figure 2 (a). The boundary condition is

$$u_t(x_b, t) = -\eta a(x_b)^2 \nabla u(x_b, t) \cdot n(x_b) - \frac{1}{C_m} g(m(x_b, t), n(x_b, t), h(x_b, t)) u(x_b, t) + \frac{1}{C_m} f(m(x_b, t), n(x_b, t), h(x_b, t), x_b, t) \quad (8)$$

with

$$\eta = \frac{\pi}{A_{\text{soma}} R_i C_m} > 0 \quad (9)$$

where A_{soma} denotes the soma surface area.

This condition can be also extended to the case of multiple cables connected to the soma. This boundary condition enforces the current conservation at the soma: the potential change at the soma results from incoming and outgoing currents from the cables connected to it, as well as the currents related to the ion channels modeled by the soma gating variables $(m(x_b, t), n(x_b, t), h(x_b, t))$. Due to its relative large size, the potential in the soma is assumed to be uniform.

Remark. Note here the similarity between the boundary equation (8) and the cable equation (1). The only difference lies in the spatial derivative term.

2.5. Junction interface conditions

When multiple cables meet at a common junction, as depicted in Figure 2 (b), appropriate interface conditions have to be applied. These conditions correspond to potential continuity and current conservation [4]. If N_c cables of respective potential $u^{(i)}$, $i = 1, \dots, N_c$ and cable radius $a^{(i)}(\cdot)$ have a junction at $x = x_b$, then these interface conditions are

$$u^{(i)}(x_b, t) = u^{(j)}(x_b, t), \quad i, j \in \{1, \dots, N_c\} \quad (10)$$

for potential continuity and

$$\sum_{i=1}^{N_c} (a^{(i)}(x_b))^2 \nabla u^{(i)}(x_b, t) \cdot n^{(i)}(x_b) = 0 \quad (11)$$

for current conservation.

2.6. Energy estimates and well-posedness

The first requirement for obtaining a reliable solution is well-posedness [20, 22]. A well-posed problem is bounded by the data of the problem and has a unique solution. Uniqueness for linear problems such as (12) below follows directly from the a priori energy estimate. Existence is motivated by using a minimal number of boundary conditions, in this case one at each end of the cable. In the rest of the paper, it is assumed that existence is not a problem and it will not be discussed further.

2.6.1. Cable and soma

The case of a single cable connected to the soma is first studied. Dropping the source terms, the cable equation is written as

$$a(x)u_t = \mu(a(x)^2u_x)_x - \frac{a(x)}{C_m}g(x,t)u, \quad (x,t) \in [0,L] \times [0,T] \quad (12)$$

where $g(x,t) = g(m(x,t), n(x,t), h(x,t)) \in [g_{\min}, g_{\max}]$ and $a(x) \in [a_{\min}, a_{\max}]$, with

$$g_{\min} = g_3 > 0, \quad g_{\max} = \sum_{i=1}^3 g_i, \quad a_{\min} > 0. \quad (13)$$

The boundary conditions associated with the cable equation are, in the case of a single cable connected to the soma at $x_b = L$,

$$u_x(0) = 0, \quad u_t(L) = -\eta a(L)^2 u_x(L) - \frac{1}{C_m} g(L,t) u(L). \quad (14)$$

Defining the energy norm of u at time t as

$$\|u\|^2 = \int_0^L u(x,t)^2 dx, \quad (15)$$

By multiplying Eq. (12) with u and integrating over the domain $[0, L]$, one obtains

$$\frac{1}{2} \|\sqrt{a}u\|_t^2 = -\|\sqrt{\mu}a u_x\|^2 + \mu(a(L)^2 u_x(L)u(L) - a(0)^2 u_x(0)u(0)) - \left\| \sqrt{\frac{ga}{C_m}} u \right\|^2. \quad (16)$$

The sealed boundary condition at $x = 0$ and the soma boundary equation at $x = L$ result in

$$\frac{1}{2} \|\sqrt{a}u\|_t^2 + \frac{\mu}{2\eta} (u^2)_t(L) = -\|\sqrt{\mu}a u_x\|^2 - \frac{\mu g(L,t)}{\eta C_m} u(L)^2 - \left\| \sqrt{\frac{ga}{C_m}} u \right\|^2. \quad (17)$$

Defining the weighted norm

$$\|u\|_*^2 = \|\sqrt{a}u\|^2 + \frac{\mu}{\eta} u(L)^2,$$

Eq. (17) becomes,

$$(\|u\|_*^2)_t + 2\|\sqrt{\mu}a u_x\|^2 + 2 \left\| \sqrt{\frac{g}{C_m}} u \right\|_*^2 = 0. \quad (18)$$

The energy estimate (18) leads directly to uniqueness by considering the difference between two solutions. By assuming that a solution exists, the following proposition summarizes the result.

Proposition 2. The initial boundary value problem (12)-(14) is well-posed.

2.6.2. Cables with junction

In this section, the case of N_c cables connected at a junction is considered. For simplification, it is assumed that all the other cable extremities are either sealed or clamped. If one of those extremities was connected to the soma, a similar approach to the one presented in the previous section can be used.

$u^{(i)}(x^{(i)}, t)$, $(x^{(i)}, t) \in [0, L^{(i)}] \times [0, T]$ here denotes the potential in the i -th cable, $i = 1, \dots, N_c$. To simplify the notations, it is assumed here that the junction is located at $x^{(i)} = 0$, all the other cable extremities being sealed, except the last one where the potential is held constant at zero. Hence, the PDEs of interest are of the same form as (12) where u , x , a and L are replaced by $u^{(i)}$, $x^{(i)}$, $a^{(i)}$ and $L^{(i)}$ respectively. The interface conditions are

$$u^{(i)}(0, t) = u^{(j)}(0, t), \quad \forall i, j = 1, \dots, N_c, \quad \sum_{i=1}^{N_c} (a^{(i)}(0))^2 u_{x^{(i)}}^{(i)}(0, t) = 0, \quad (19)$$

$$u_{x^{(i)}}^{(i)}(L^{(i)}, t) = 0, \quad i = 1, \dots, N_c - 1 \quad (20)$$

and

$$u^{(N_c)}(L^{(N_c)}, t) = 0. \quad (21)$$

The energy norm for $u^{(i)}$ at time t is defined in (15) where the integral bounds are 0 and $L^{(i)}$.

For each cable $i \in 1, \dots, N_c$ equation (16) holds with appropriate variables. Summing those equations and applying the sealed end and voltage clamp boundary conditions leads to

$$\begin{aligned} \frac{1}{2} \sum_{i=1}^{N_c} \left\| \sqrt{a^{(i)}} u^{(i)} \right\|_t^2 &= -\mu \sum_{i=1}^{N_c} \left\| a^{(i)} u_{x^{(i)}}^{(i)} \right\|^2 - \mu \sum_{i=1}^{N_c} (a^{(i)}(0))^2 u_{x^{(i)}}^{(i)}(0) u^{(i)}(0) \\ &\quad - \sum_{i=1}^{N_c} \left\| \sqrt{\frac{g^{(i)} a^{(i)}}{C_m}} u^{(i)} \right\|^2. \end{aligned} \quad (22)$$

Applying the potential continuity condition at the junction, $u^{(1)}(0) = u^{(i)}(0)$, $i = 2, \dots, N_c$, the identity

$$\sum_{i=1}^{N_c} (a^{(i)}(0))^2 u_{x^{(i)}}^{(i)}(0) u^{(i)}(0) = u^{(1)}(0) \sum_{i=1}^{N_c} (a^{(i)}(0))^2 u_{x^{(i)}}^{(i)}(0) \quad (23)$$

and the current conservation at the junction leads to cancelation of the second factor in the right hand side of equality (22). Hence

$$\frac{1}{2} \sum_{i=1}^{N_c} \left\| \sqrt{a^{(i)}} u^{(i)} \right\|_t^2 = -\mu \sum_{i=1}^{N_c} \left\| a^{(i)} u_{x^{(i)}}^{(i)} \right\|^2 - \sum_{i=1}^{N_c} \left\| \sqrt{\frac{g^{(i)} a^{(i)}}{C_m}} u^{(i)} \right\|^2. \quad (24)$$

One can define the weighted norm $\|\cdot\|_*$ for $u = [u^{(1)}, \dots, u^{(N_c)}]^T$ as

$$\|u\|_*^2 = \sum_{i=1}^{N_c} \left\| \sqrt{a^{(i)}} u^{(i)} \right\|^2. \quad (25)$$

The energy equality then becomes

$$(\|u\|_*^2)_t + 2\|\sqrt{\mu a} u_x\|_*^2 + 2\left\| \sqrt{\frac{g}{C_m}} u \right\|_*^2 = 0. \quad (26)$$

As in the previous section, the energy estimate (26) leads to uniqueness and by assuming existence (the right number of boundary conditions), the following proposition summarizes the result.

Proposition 3. The initial boundary value problem (12), (19), (20), (21) holding for N_c cables connected at a junction and with other cable extremities sealed or clamped is well-posed.

3. The semi-discrete problem

In this section, Eq. (12) is discretized on the domain $[0, L]$ using a uniform mesh of $N + 1$ points. The discrete approximation of $u(\cdot, t)$ is

$$\mathbf{u}(t) = [u_0(t), \dots, u_N(t)]^T, \quad u_i(t) \approx u\left(\frac{i-1}{N}L, t\right), \quad i = 1, \dots, N.$$

Operators of SBP form [20] approximate the derivative of $u(\cdot, t)$ as

$$\mathbf{u}_x(t) = [u_{x0}(t), \dots, u_{xN}(t)]^T = \mathbf{D}_1 \mathbf{u}(t) = \mathbf{P}^{-1} \mathbf{Q} \mathbf{u}(t), \quad (27)$$

where \mathbf{P} is a diagonal symmetric positive definite matrix and \mathbf{Q} satisfies $\mathbf{Q} + \mathbf{Q}^T = \mathbf{B} = \mathbf{diag}(-1, 0, \dots, 0, 1)$. The space derivative $(a(x)^2 u_x)_x$ in this paper is approximated as

$$\mathbf{D}_1(\mathbf{A}^2 \mathbf{D}_1 \mathbf{u}(t)) = (\mathbf{P}^{-1} \mathbf{Q}) \mathbf{A}^2 (\mathbf{P}^{-1} \mathbf{Q}) \mathbf{u}(t), \quad (28)$$

where the diagonal matrix $\mathbf{A} = \mathbf{diag}(a_0, \dots, a_N)$ with $a_j = a\left(\frac{j-1}{N}L\right)$, $j = 1, \dots, N$. Compact second derivatives in second order form also exist [12, 21].

To alleviate notations, the dependency of \mathbf{u} and its derivatives on time is omitted in the following. A norm based on \mathbf{P} is

$$\|\mathbf{u}\| = \sqrt{\mathbf{u}^T \mathbf{P} \mathbf{u}}. \quad (29)$$

The semi-discrete version of (12) without inclusion of boundary conditions is

$$\mathbf{A} \mathbf{u}_t = \mu \mathbf{P}^{-1} \mathbf{Q} (\mathbf{A}^2 \mathbf{u}_x) - \frac{1}{C_m} \mathbf{A} \mathbf{G}(t) \mathbf{u} \quad (30)$$

where the diagonal matrix $\mathbf{G}(t) = \mathbf{diag}(g_0(t), \dots, g_N(t))$ with $g_j(t) = g\left(\frac{j-1}{N}L, t\right)$, $j = 1, \dots, N$.

3.1. Cable with soma

The boundary conditions (14) are integrated in the formulation as penalty terms in the following way

$$\begin{aligned} \mathbf{A} \mathbf{u}_t &= \mu \mathbf{P}^{-1} \mathbf{Q} (\mathbf{A}^2 \mathbf{u}_x) - \frac{1}{C_m} \mathbf{A} \mathbf{G}(t) \mathbf{u} + \sigma_0 \mathbf{P}^{-1} (u_{x0} - 0) \mathbf{e}_0 \\ &+ \sigma_L \mathbf{P}^{-1} \left(u_{tN} + \eta a_N^2 u_{xN} + \frac{1}{C_m} g_N(t) u_N - 0 \right) \mathbf{e}_L, \end{aligned} \quad (31)$$

where, for clarity, the data is indicated by 0.

Premultiplying Eq. (31) by $\mathbf{u}^T \mathbf{P}$ leads to

$$\begin{aligned} \mathbf{u}^T \mathbf{P} \mathbf{A} \mathbf{u}_t &= \mu \mathbf{u}^T \mathbf{Q} (\mathbf{A}^2 \mathbf{u}_x) - \frac{1}{C_m} \mathbf{u}^T \mathbf{P} \mathbf{A} \mathbf{G}(t) \mathbf{u} + \sigma_0 u_{x0} u_0 \\ &+ \sigma_L u_N \left(u_{tN} + \eta a_N^2 u_{xN} + \frac{1}{C_m} g_N(t) u_N \right) \end{aligned} \quad (32)$$

Since \mathbf{P} , \mathbf{A} and $\mathbf{G}(t)$ are diagonal matrices, they commute and lead to

$$\frac{1}{C_m} \mathbf{u}^T \mathbf{P} \mathbf{A} \mathbf{G}(t) \mathbf{u} = \mathbf{u}^T \sqrt{\frac{\mathbf{G}(t) \mathbf{A}}{C_m}} \mathbf{P} \sqrt{\frac{\mathbf{G}(t) \mathbf{A}}{C_m}} \mathbf{u} = \left\| \sqrt{\frac{\mathbf{G}(t) \mathbf{A}}{C_m}} \mathbf{u} \right\|^2, \quad (33)$$

$$\mathbf{u}^T \mathbf{P} \mathbf{A} \mathbf{u}_t = \mathbf{u}^T \sqrt{\mathbf{A} \mathbf{P}} \sqrt{\mathbf{A}} \mathbf{u}_t = \frac{1}{2} \|\sqrt{\mathbf{A}} \mathbf{u}\|_t^2. \quad (34)$$

The SBP properties lead to

$$\begin{aligned}
\mathbf{u}^T \mathbf{Q}(\mathbf{A}^2 \mathbf{u}_x) &= \mathbf{u}^T (\mathbf{B} - \mathbf{Q}^T) \mathbf{P}^{-1} \mathbf{P}(\mathbf{A}^2 \mathbf{u}_x) \\
&= -\mathbf{u}^T (\mathbf{P}^{-1} \mathbf{Q})^T \mathbf{P}(\mathbf{A}^2 \mathbf{u}_x) + \mathbf{u}^T \mathbf{B}(\mathbf{A}^2 \mathbf{u}_x) \\
&= -\mathbf{u}_x^T \mathbf{P}(\mathbf{A}^2 \mathbf{u}_x) - a_0^2 u_0 u_{x0} + a_N^2 u_N u_{xN} \\
&= -\|\mathbf{A} \mathbf{u}_x\|^2 + a_N^2 u_N u_{xN} - a_0^2 u_0 u_{x0}.
\end{aligned} \tag{35}$$

By the choice $\sigma_0 = \mu a_0^2$ and $\sigma_L = -\frac{\mu}{\eta}$, Eq. (32) becomes

$$\frac{1}{2} \|\sqrt{\mathbf{A}} \mathbf{u}\|_t^2 = -\mu \|\mathbf{A} \mathbf{u}_x\|^2 - \left\| \sqrt{\frac{\mathbf{G}(t) \mathbf{A}}{C_m}} \mathbf{u} \right\|^2 - \frac{\mu}{\eta} u_N \left(u_{tN} + \frac{1}{C_m} g_N(t) u_N \right). \tag{36}$$

Similarly as in the continuous case, one can define a weighted norm

$$\|\mathbf{u}\|_*^2 = \|\sqrt{\mathbf{A}} \mathbf{u}\|^2 + \frac{\mu}{\eta} u_N^2, \tag{37}$$

which leads following energy estimate and proposition

$$\|\mathbf{u}\|_{*,t}^2 + 2\mu \|\mathbf{A} \mathbf{u}_x\|^2 + 2 \left\| \sqrt{\frac{\mathbf{G}(t)}{C_m}} \mathbf{u} \right\|_*^2 = 0. \tag{38}$$

Proposition 4. The SBP-SAT scheme (31) for solving the semi-discrete problem associated with the cable equation with soma as a boundary condition is stable [20, 22].

Remark. Note that the energy estimate (38) is the semi-discrete analog to the continuous energy estimate (18) derived in Section 2.6.1.

3.2. Cables with junction

Each cable is here discretized on the domain $[0, L^{(i)}]$, $i = 1, \dots, N_c$ using a uniform mesh of $N^{(i)} + 1$ points. One defines the discrete approximation of $u^{(i)}(\cdot, t)$, $i = 1, \dots, N_c$ as

$$\mathbf{u}^{(i)}(t) = \left[u_0^{(i)}(t), \dots, u_{N^{(i)}}^{(i)}(t) \right]. \tag{39}$$

The space derivatives of $\mathbf{u}^{(i)}(t)$ are approximated as

$$\mathbf{u}_x^{(i)}(t) = \left(\mathbf{P}^{(i)} \right)^{-1} \mathbf{Q}^{(i)} \mathbf{u}^{(i)}(t), \tag{40}$$

where $(\mathbf{P}^{(i)}, \mathbf{Q}^{(i)})$, $i = 1, \dots, N_c$ have similar properties as in the previous section. Diagonal matrices $\mathbf{A}^{(i)}$, $\mathbf{G}^{(i)}(t)$ are defined as in the previous section. Similarly as in the previous section, the dependency of \mathbf{u} and its derivatives on time is omitted for clarity. The semi-discretized equations are all of the same form as (30).

The interface conditions (19)–(21) are added as penalty terms, resulting in

$$\begin{aligned}
\mathbf{A}^{(i)} \mathbf{u}_t^{(i)} &= \mu^{(i)} \left(\mathbf{P}^{(i)} \right)^{-1} \mathbf{Q}^{(i)} \left(\left(\mathbf{A}^{(i)} \right)^2 \mathbf{u}_x^{(i)} \right) - \frac{1}{C_m} \mathbf{A}^{(i)} \mathbf{G}^{(i)}(t) \mathbf{u}^{(i)} \\
&+ \sum_{j=1, j \neq i}^{N_c} \sigma_{0,j}^{(i)} \left(\mathbf{P}^{(i)} \right)^{-1} \left(\mathbf{D}_1^{(i)} \right)^T \left(u_0^{(i)} - u_0^{(j)} \right) \mathbf{e}_0^{(i)} \\
&+ \sigma_{0,i}^{(i)} \left(\sum_{j=1}^{N_c} (a_0^{(j)})^2 u_{x0}^{(j)} - 0 \right) \left(\mathbf{P}^{(i)} \right)^{-1} \mathbf{e}_0^{(i)} \\
&+ p_L^{(i)}, \quad i = 1, \dots, N_c,
\end{aligned} \tag{41}$$

where $p_L^{(i)}$ denotes the penalty term for the i -th cable associated with the boundary $x = L^{(i)}$:

$$p_L^{(i)} = \sigma_L^{(i)} \left(\mathbf{P}^{(i)} \right)^{-1} \left(u_{xN^{(i)}}^{(i)} - 0 \right) \mathbf{e}_L^{(i)}, \quad i = 1, \dots, N_i - 1 \quad (42)$$

for the sealed boundary conditions $u_{xN^{(i)}}^{(i)} = 0$, and

$$p_L^{(N_c)} = \sigma_L^{(N_c)} \left(\mathbf{P}^{(N_c)} \right)^{-1} \left(\mathbf{D}_1^{(N_c)} \right)^T \left(u^{(N_c)} - 0 \right) \mathbf{e}_L^{(N_c)} \quad (43)$$

for the voltage clamp condition $u^{(N_c)} = 0$. These penalty terms can be all recast in the same form

$$p_L^{(i)} = \sigma_L^{(i)} \left(\mathbf{P}^{(i)} \right)^{-1} u_{xN^{(i)}}^{(i)} \mathbf{e}_L^{(i)}, \quad i = 1, \dots, N_i. \quad (44)$$

Multiplying by $(\mathbf{u}^{(i)})^T \mathbf{P}^{(i)}$ and using analog identities to the one derived in the previous section leads to

$$\begin{aligned} \frac{1}{2} \left\| \sqrt{\mathbf{A}^{(i)}} \mathbf{u}^{(i)} \right\|_t^2 &= -\mu \left\| \mathbf{A}^{(i)} \mathbf{u}_x^{(i)} \right\|^2 - \left\| \sqrt{\frac{\mathbf{G}^{(i)}(t) \mathbf{A}^{(i)}}{C_m}} \mathbf{u}^{(i)} \right\|^2 \\ &+ \sum_{j=1, j \neq i}^{N_c} \sigma_{0,j}^{(i)} u_{x0}^{(i)} \left(u_0^{(i)} - u_0^{(j)} \right) \\ &+ \sigma_{0,i}^{(i)} \sum_{j=1, j \neq i}^{N_c} (a_0^{(j)})^2 u_0^{(i)} u_{x0}^{(j)} \\ &+ (\sigma_{0,i}^{(i)} - \mu) (a_0^{(i)})^2 u_0^{(i)} u_{x0}^{(i)} \\ &+ (\sigma_L^{(i)} + \mu (a_{N^{(i)}}^{(i)})^2) u_{xN^{(i)}}^{(i)} u_{N^{(i)}}^{(i)}, \quad i = 1, \dots, N_c. \end{aligned} \quad (45)$$

Summing the N_c equalities (45) and choosing the penalty coefficients $\sigma_L^{(i)} = -\mu \left(a_{N^{(i)}}^{(i)} \right)^2$,

$$\sigma_{0,i}^{(i)} = \frac{\mu}{N_c}, \quad i = 1, \dots, N_c \quad (46)$$

and

$$\sigma_{0,i}^{(j)} = \sigma_{0,i}^{(i)} (a_0^{(j)})^2 = \frac{\mu}{N_c} (a_0^{(j)})^2 \quad (47)$$

leads to the energy estimate

$$\frac{1}{2} \sum_{i=1}^{N_c} \left\| \sqrt{\mathbf{A}^{(i)}} \mathbf{u}^{(i)} \right\|_t^2 = -\mu \sum_{i=1}^{N_c} \left\| \mathbf{A}^{(i)} \mathbf{u}_x^{(i)} \right\|^2 - \sum_{i=1}^{N_c} \left\| \sqrt{\frac{\mathbf{G}^{(i)}(t) \mathbf{A}^{(i)}}{C_m}} \mathbf{u}^{(i)} \right\|^2. \quad (48)$$

Defining the weighted norm

$$\|\mathbf{u}\|_*^2 = \sum_{i=1}^{N_c} \left\| \sqrt{\mathbf{A}^{(i)}} \mathbf{u}^{(i)} \right\|^2, \quad (49)$$

the following energy equality holds as well as the proposition

$$\left(\|\mathbf{u}\|_*^2 \right) + 2\mu \left\| \sqrt{\mathbf{A}} \mathbf{u} \right\|_*^2 + 2 \left\| \sqrt{\frac{\mathbf{G}(t)}{C_m}} \mathbf{u} \right\|_*^2 = 0. \quad (50)$$

Proposition 5. The SBP-SAT scheme for solving the semi-discrete problem (41) associated with the initial boundary value problem (12), (19), (20), (21) is stable.

Remark. Note that this energy estimate is the exact semi-discrete analog to the energy equality (26) derived in Section 2.6.2.

4. Order of convergence

The method of manufactured solutions [23] is used to determine the discretization order. For the two problems mentioned above, a closed form solution is chosen and appropriate source terms are added to the initial boundary value problem of interest so that the closed form solution satisfies it. Time integration is done using the fourth-order explicit Runge-Kutta scheme and a time step of $\Delta t = 10^{-9}$ s, ensuring that the time discretization errors are negligible. The accuracy of the discretization is defined as the minimal order of the local truncation error and the convergence rate is calculated as

$$q = \frac{\log_{10} \left(\frac{\|\mathbf{v}_{h_1} - \mathbf{u}\|}{\|\mathbf{v}_{h_2} - \mathbf{u}\|} \right)}{\log_{10} \left(\frac{h_1}{h_2} \right)}. \quad (51)$$

4.1. Cables with junction

Three cables with junction at $x^{(i)} = 0$, $i = 1, \dots, 3$ are considered. Their respective cable radii are constant for each cable. The exact manufactured solutions $u^{(i)}(x, t)$, $i = 1, \dots, 3$ and their corresponding initial boundary value problem are specified in Appendix C. The physical constants associated with the problems are reported in Tables 1 and 2. The exact solutions $u^{(i)}(x, t)$ at times $t = 0$ and $t = T$ are plotted in Figure 3.

Specific membrane capacitance	C_m	10^{-2} F.m $^{-2}$
Axial Resistivity	R_i	0.354 ohm.m
Conductance	g_1	1200 ohm $^{-1}$.m $^{-2}$
Conductance	g_2	360 ohm $^{-1}$.m $^{-2}$
Conductance	g_3	3 ohm $^{-1}$.m $^{-2}$
Equilibrium potential	E_1	0.115 V
Equilibrium potential	E_2	-0.012 V
Equilibrium potential	E_3	0.010613 V

Table 1 Physical constants for the problems of interest

Cable length	$L^{(1)}$	0.05 m
Cable length	$L^{(2)}$	0.05 m
Cable length	$L^{(3)}$	0.063 m
Cable radius	$a^{(1)}(x)$	0.476×10^{-3} m
Cable radius	$a^{(2)}(x)$	0.476×10^{-3} m
Cable radius	$a^{(3)}(x)$	0.7556×10^{-3} m

Table 2 Geometric parameters associated with the junction problem

The solutions $u^{(i)}(x^{(i)}, t)$ at $t = 0$ and $t = T$ are reported in Figure 3.

The convergence results are reported in Table 3 and Figure 4. The slopes corresponding to each operators order are also shown in Figure 4. Second-order convergence is observed with second-order operators, third-order convergence with third-order operators, fourth-order convergence with fourth-order operators and fifth-order convergence with fifth-order operators. When reaching machine precision, the convergence orders decrease as expected.

The CPU times associated with each computation are reported in Table 4. The CPU times corresponding to a relative error of the order of 10^{-6} are also highlighted in bold font. For a given number of grid points, the second-order operators are less computationally costly than the higher-order operators. However, for the same accuracy, the CPU time associated with the second-order operators is 4.5 times larger than the ones

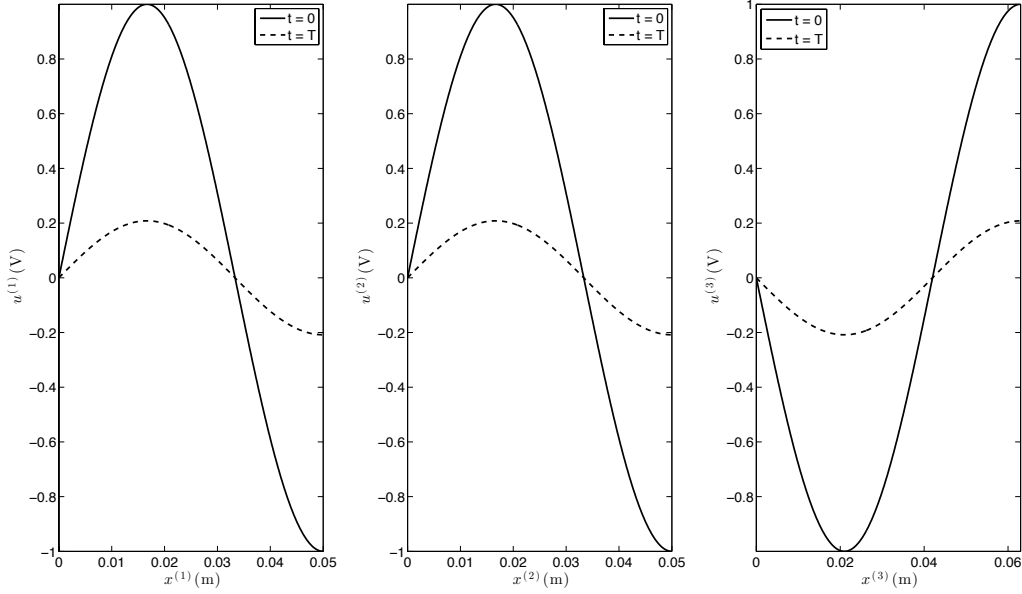


Figure 3 Exact solutions for the junction problem

associated with the higher-order operators. As a result, the higher-order methods are more efficient than their second-order counterpart.

N	order 2	order 3	order 4	order 5
32	0.707003	1.359596	2.381819	3.028414
64	0.969357	2.641288	3.757290	5.092958
128	2.135884	3.319466	3.876460	4.843739
256	2.099840	3.097754	4.138360	4.951223
512	2.051456	3.043053	4.327195	5.108929
1024	2.026236	3.021139	4.385053	4.148390
2048	2.013295	3.010569	2.279472	-3.273673

Table 3 Numerical convergence behavior for each operator choice

4.2. Cable and soma

The exact manufactured solution $u(x, t)$ and the corresponding initial boundary value problem are specified in Appendix D. The physical constants associated with the problem are reported in Tables 1 and 5. The exact solutions $u(x, t)$ at times $t = 0$ and $t = T$ are depicted in Figure 5.

The convergence results are reported in Table 6 and Figure 6, in which slopes corresponding to the operators orders are also depicted. Second-order convergence can be observed using second-order operators, fourth order convergence is observed when using third- and fourth-order operators and fifth-order convergence for fifth-order operators. Again, when reaching machine precision, the convergence orders decrease. Unlike the numerical experiments performed for the junction problem, for which third-order convergence was found, in the present case, a better convergence rate is found for third-order operators. The authors of this paper have observed this surprising phenomenon in the past for other problems, probably due to a vanishing

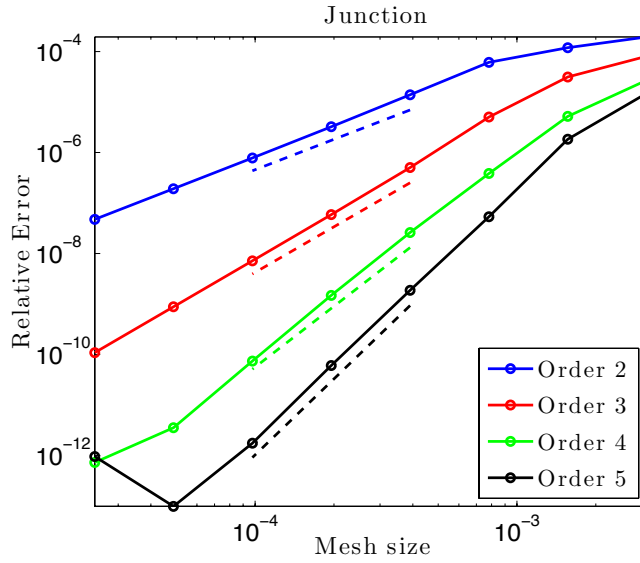


Figure 4 Errors in function of mesh size and operators order for the junction problem

N	order 2	order 3	order 4	order 5
16	28.97	29.16	29.14	28.37
32	27.10	28.16	31.59	27.94
64	27.95	31.16	29.77	31.62
128	30.85	32.89	32.32	32.70
256	32.36	35.69	36.96	40.33
512	86.18	100.56	111.98	116.86
1024	108.52	138.75	159.95	169.15
2048	157.47	226.92	267.26	304.23

Table 4 CPU times (in seconds) for each operator choice in the junction problem

Cable length	L	0.05 m
Cable radius	$a(x)$	0.476×10^{-3} m
Soma radius	r_{soma}	2×10^{-3} m

Table 5 Geometric parameters associated with the cable with soma problem

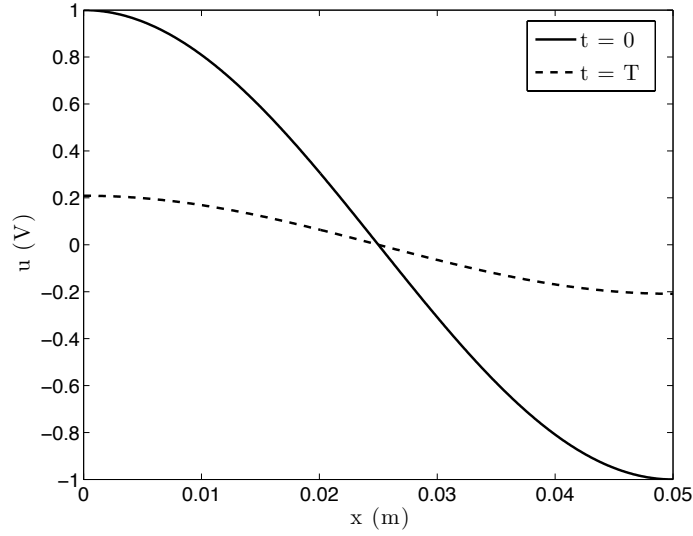


Figure 5 Exact solutions for the cable with soma problem

coefficient multiplying the corresponding error term. For this case, no real advantage can be seen in terms of using fourth-order operators over third-order operators, since the corresponding errors are comparable.

The CPU times associated with each computation are reported in Table 7. In that table, the CPU times corresponding to a relative error of the order of 5×10^{-7} are highlighted in bold font. Note that for the same accuracy, the CPU time associated with the second-order operators is 7.5 times larger than the ones associated with the high-order operators.

N	order 2	order 3	order 4	order 5
32	0.766683	2.862748	2.567863	4.554248
64	1.345940	3.386744	3.004467	4.927776
128	1.978948	3.752389	3.588062	5.442091
256	2.005454	3.962842	4.090079	5.691623
512	2.000201	3.983892	4.314146	5.161448
1024	2.000000	3.945898	4.385063	1.286661
2048	2.000000	3.852652	4.355057	-1.309231
4096	2.000000	0.537888	0.524158	-1.901695

Table 6 Numerical convergence behavior for each operator choice

5. Numerical applications

5.1. Time discretization

After space discretization by the approach developed in this paper, the Hodgkin-Huxley equations become a set of coupled ODEs of the form

$$\begin{aligned} \frac{d\mathbf{u}}{dt} &= \mathbf{A}_1(\mathbf{w})\mathbf{u} + \mathbf{b}_1(\mathbf{w}, t) \\ \frac{d\mathbf{w}}{dt} &= \mathbf{A}_2(\mathbf{u})\mathbf{w} + \mathbf{b}_2(\mathbf{u}) \end{aligned}$$

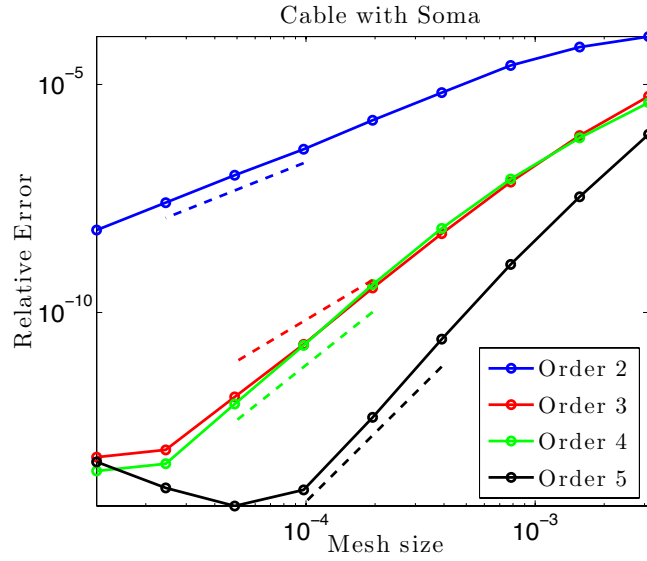


Figure 6 Errors in function of mesh size and operators order for the cable attached to soma problem

N	order 2	order 3	order 4	order 5
16	6.35	6.36	6.33	6.21
32	6.38	6.42	6.54	6.39
64	6.51	6.54	7.20	6.47
128	6.73	6.73	7.15	6.72
256	7.07	7.17	7.35	7.13
512	7.75	7.9	8.1	8.01
1024	9.16	9.45	9.78	9.66
2048	27.15	28.26	30.01	28.9
4096	52.90	56.6	59.13	61.32

Table 7 CPU times (in seconds) for each operator choice in the cable attached to soma problem

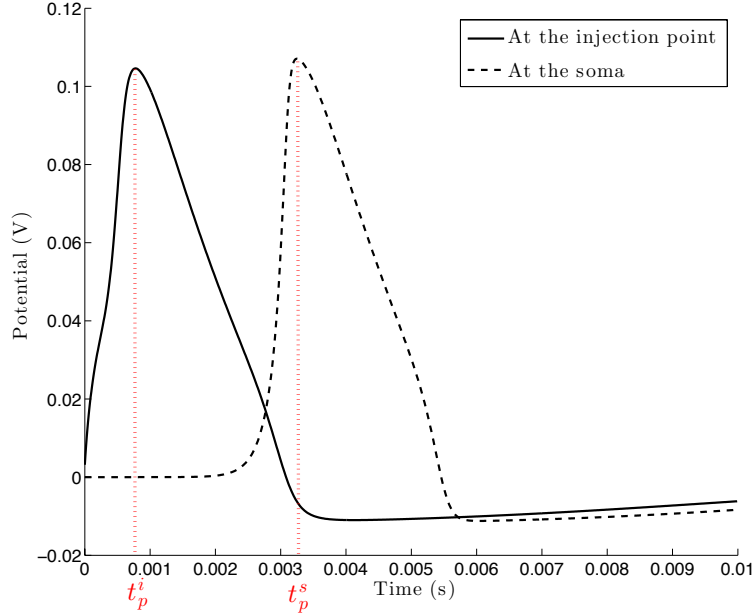


Figure 7 Action potential at the current injection point and the soma obtained using fifth-order operators

where the discrete variables for the potential and gating variables are $\mathbf{u} \in \mathbb{R}^{N+1}$ and $\mathbf{w} = [\mathbf{m}, \mathbf{h}, \mathbf{n}]^T \in \mathbb{R}^{3(N+1)}$, respectively.

This set of coupled ODEs is then discretized in time, using the second-order implicit Crank-Nicolson staggered difference scheme initially developed by Hines [3]. The scheme is

$$\begin{aligned} \left(\mathbf{I} - \frac{\Delta t}{2} \mathbf{A}_2(\mathbf{u}^n) \right) \mathbf{w}^{n+\frac{1}{2}} &= \left(\mathbf{I} + \frac{\Delta t}{2} \mathbf{A}_2(\mathbf{u}^n) \right) \mathbf{w}^{n-\frac{1}{2}} + \Delta t \mathbf{b}_2(\mathbf{u}^n) \\ \left(\mathbf{I} - \frac{\Delta t}{2} \mathbf{A}_1(\mathbf{w}^{n+\frac{1}{2}}) \right) \mathbf{u}^{n+1} &= \left(\mathbf{I} + \frac{\Delta t}{2} \mathbf{A}_1(\mathbf{w}^{n+\frac{1}{2}}) \right) \mathbf{u}^n + \Delta t \mathbf{b}_1(\mathbf{w}^{n+\frac{1}{2}}, t^{n+\frac{1}{2}}). \end{aligned}$$

Here $\mathbf{u}^n \approx \mathbf{u}(t^n) = \mathbf{u}(n\Delta t)$ and $\mathbf{w}^{n+\frac{1}{2}} \approx \mathbf{w}(t^{n+\frac{1}{2}}) = \mathbf{w}\left(\left(n + \frac{1}{2}\right)\Delta t\right)$.

Remark. The set of coupled ODEs was found to be too stiff for the fourth-order Runge-Kutta scheme used in the previous sections. This motivates the choice of an implicit scheme that allows for arbitrary large time-steps. Even though this time integration scheme is only second-order accurate, it was consistently found in the numerical experiments that the space error term was dominating the time error term.

5.2. Potential propagation in a cable attached to the soma

The physical constants associated with this problem are provided in Table 1. These correspond to the giant squid's axon studied by Hodgkin and Huxley in [1]. The expressions for the gating functions are provided in Appendix A.

Current with Gaussian distribution and maximum intensity $I = 10$ nA is injected at the top extremity of the cable depicted in Figure 2(a) and the cable potential time history for $t = [0, 10]$ ms is recorded at the two extremities of the cable. The corresponding time histories obtained by applying the procedure developed in this paper with $N = 32$ and 5-th order differential operators and a time step size of $dt = 10^{-2}$ ms are reported in Figure 7. The typical action potential characteristic shape [19] can be observed.

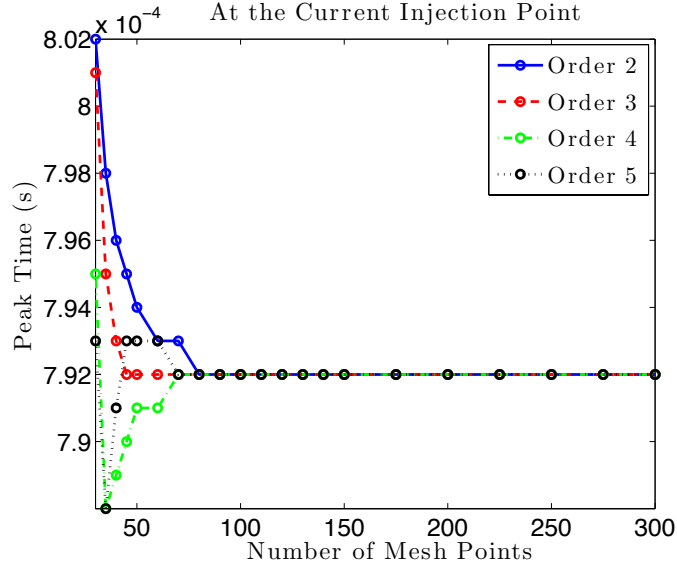


Figure 8 Action potential peak times t_p^i at the current injection point

Next, the action potential peak times obtained at the two extremities of the cable of interest are recorded and shown for various choices of order for the differential operators and various numbers of mesh points. The peak time at the injection points t_p^i , depicted in Figure 7, are almost identical as it can be observed in Figure 8. However, for coarse meshes, second-order operators result in an inaccurate peak time t_p^s at the Soma, as observed in Figure 9. This results in inaccurate propagation times for these coarse meshes when second-order operators are used, whereas the propagations times are accurate with high-order operators even when using those coarse meshes, as shown in Figure 10.

5.3. Potential propagation in a dendritic network

In order to illustrate the capability of the proposed approach to predict potential propagation in large dendritic networks, a tree with 15 branches attached to the soma, as depicted in Figure 11, is considered. The dimensions of each branch in the tree are chosen according to Rall's 3/2 power law [2] and correspond to Rallpack's second configuration [24]. The cable lengths and radii at each level of the tree are reported in Table 8. All the other physical constants are identical as in the previous numerical experiments. Synaptic current input is modeled by a current injection of amplitude $I = 500$ nA for a duration of 1 ms at the extremity of each of the 8 extremal branches. Each branch is discretized using 31 nodes, resulting in 1860 degrees of freedom. Fifth order difference operators are here used. The potential propagation is subsequently simulated in the entire tree in the time interval for $t \in [0, 0.2]$ s using a time step $\Delta t = 10^{-4}$ s. The entire simulation takes about 14 s CPU time when performed with MATLAB running on a Mac Book Pro 2.9 GHz Intel Core i7, 8GB 1600 MHz DDR3.

Two current input configurations are considered. The first one is depicted in Figure 12 (a). In that figure, the interval of duration 1 ms, at which a given branch input is active, is represented by a line segment. The corresponding potential recorded at the soma is reported in Figure 12 (b). There are eight characteristic action potential spikes, each one corresponding to a specific extremal branch input.

The second numerical experiment is carried out with the current input activity reported in Figure 13 (a). In this case, the current input is limited to the time interval $t \in [0, 0.1]$ s. The associated potential at the soma is presented in Figure 13 (b). Only four characteristic action potential spikes are propagated from the extremity branches of the tree to the soma. This numerical experimental emphasizes the nonlinear nature of the Hodgkin-Huxley equations. It also illustrates the concept of refractory period for action potentials

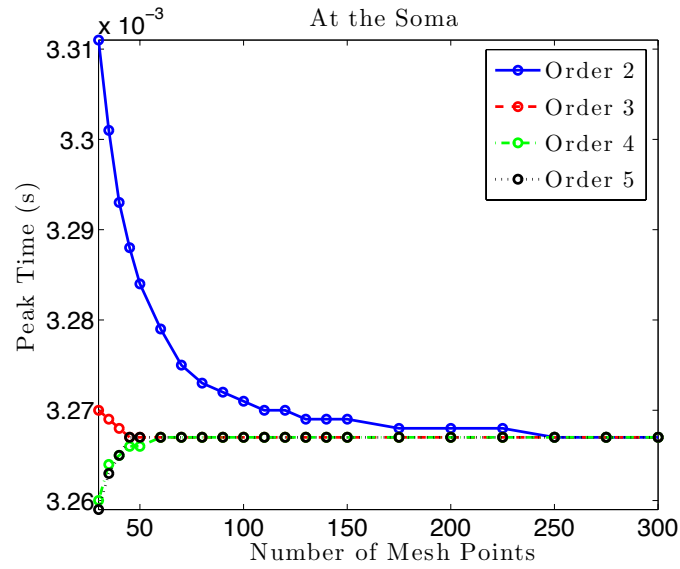


Figure 9 Action potential peak times t_p^s at the soma

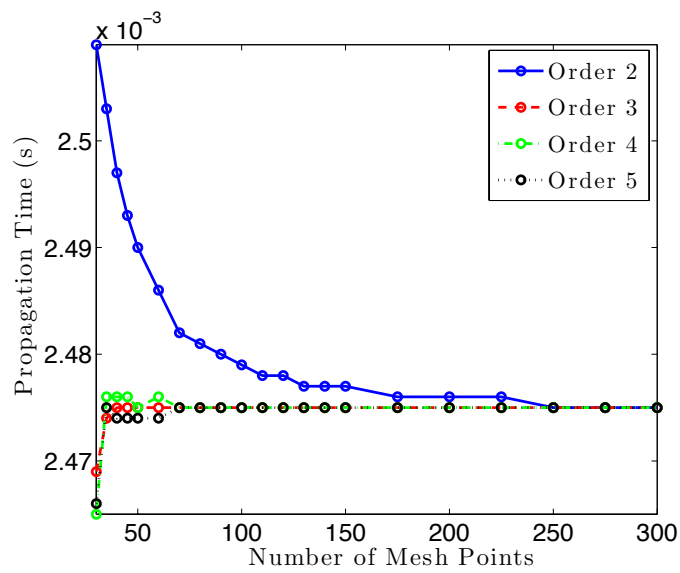


Figure 10 Propagation times from the current injection point to the soma

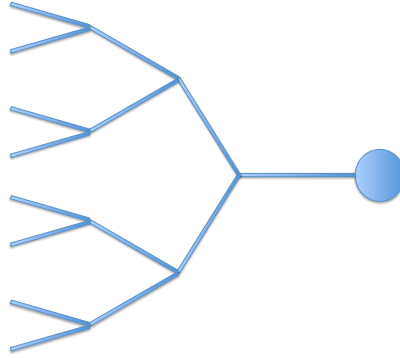


Figure 11 Dendritic tree connected to the soma

observed in neurons [25]: after an action potential has been generated, the membrane is hyper-polarized and there is a minimal period of time after which another action potential can be created. In the second numerical experiment, although eight current inputs were injected, four failed to create full-amplitude spikes since their respective injection times were within the refractory periods of the four action potentials. A small spike can also be observed around $t = 0.017$ s, but it is not a full action potential. In the first experiment, however, the time between two current injections is longer, leading to eight spikes.

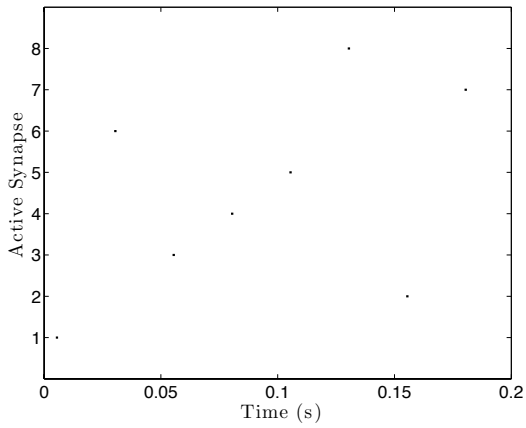
Level	Number of branches	Branch length (m)	Branch radius (m)
1	1	32.0×10^{-6}	8.0×10^{-6}
2	2	25.4×10^{-6}	5.04×10^{-6}
3	4	20.16×10^{-6}	3.18×10^{-6}
4	8	16.0×10^{-6}	2.0×10^{-6}

Table 8 Dimensions of each branch in the dendritic tree

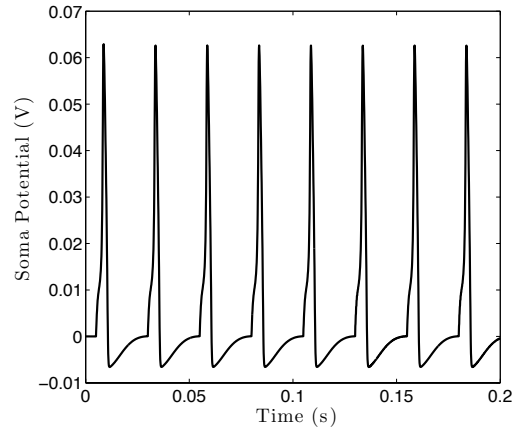
6. Conclusions

Stable and accurate high-order schemes based on Summation-By-Parts (SBP) form with the weak Simultaneous Approximation Term (SAT) procedure for boundary and interface conditions are developed for the Hodgkin-Huxley equations. These schemes are shown in this paper to be easily applicable to neuronal systems constituted of multiple branches such as in the case of dendritic trees. Well-posedness of the continuous problem as well as energy estimates are established for dendritic trees connected to the soma. The SBP-SAT procedure leads to an energy estimate and proof of stability of the discrete scheme.

Convergence and order of accuracy are illustrated on model problems. Important gains in CPU times for a given level of accuracy are also demonstrated when high-order operators are used. The superiority of high-order operators is also illustrated on a simple problem constituted of a cable connected to the soma. Finally, the proposed approach is applied to a realistic dendritic tree configuration constituted of 15 cables connected to the soma. On that configuration, the nonlinearity properties of the Hodgkin-Huxley equations are numerically demonstrated.

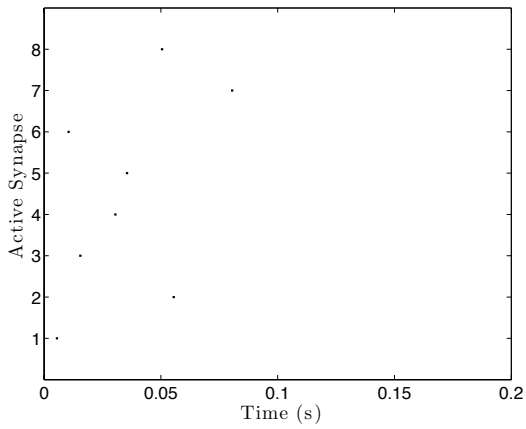


(a) Current input activity for each of the extremal branches (each line segment is of length 1 ms)

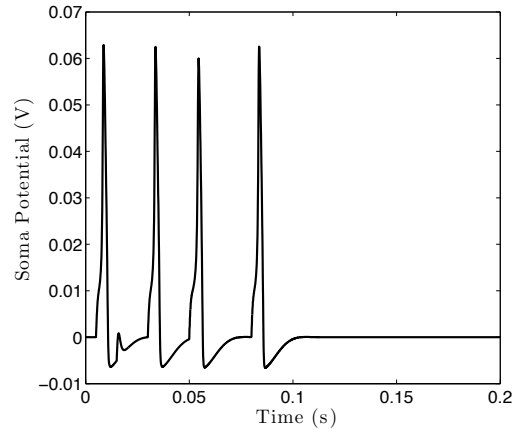


(b) Action potential at the soma

Figure 12 Potential propagation in the network for the first current input configuration



(a) Current input activity for each of the extremal branches (each line segment is of length 1 ms)



(b) Action potential at the soma

Figure 13 Potential propagation in the network for the second current input configuration

Appendix A: expressions for the gating functions

The expressions for the coefficients α_m , α_h , α_n , β_m , β_h and β_n were determined for the giant squid axon by Hodgkin and Huxley [1] as:

$$\begin{aligned}\alpha_m(u) &= \frac{10^5(0.025 - u)}{e^{\frac{0.025-u}{0.01}} - 1}, & \beta_m(u) &= 4 \times 10^3 e^{-\frac{u}{0.018}} \\ \alpha_h(u) &= 70e^{-\frac{u}{0.02}}, & \beta_h(u) &= \frac{10^3}{e^{\frac{0.03-u}{0.01}} + 1} \\ \alpha_n(u) &= \frac{10^4(0.01 - u)}{e^{\frac{0.01-u}{0.010}} - 1}, & \beta_n(u) &= 125e^{-\frac{u}{0.08}}.\end{aligned}\tag{52}$$

Appendix B: proof of proposition 1

The differential equations associated with $m(x, t)$ are a set of uncoupled ODEs for each x . As a result, it is sufficient to consider one of those ODE only for $x_0 \in [0, L]$:

$$m_t(x_0, t) = \alpha_m(u(x_0, t))(1 - m(x_0, t)) - \beta_m(u(x_0, t))m(x_0, t), \quad t \in [0, T].\tag{53}$$

To simplify the notations, in the rest of this section, the dependency on x_0 is dropped: $\alpha_m(u(x_0, t)) = \alpha_m(u(t))$, $\beta_m(u(x_0, t)) = \beta_m(u(t))$ and $m(x_0, t) = m(t)$.

From the expressions of α_m and β_m given in Appendix 1, it can be shown that

$$\alpha_m(0) > 0, \quad \beta_m(1) > 0.\tag{54}$$

These properties also hold for α_h , α_n , β_h and β_n .

An initial condition $m(0) \in [0, 1]$ is then considered. Assume that there exists $t_1 \in (0, T]$ such that $m(t_1) > 1$. As $m(\cdot)$ is continuous, this means that there exists $0 < t_0 < t_1 < T$ such that $m(t_0) = 1$ and $m(t_0 + \epsilon) > 1$, $\forall 0 < \epsilon \leq t_1 - t_0$. Since

$$\frac{dm}{dt}(t_0) = \alpha_m(u(t_0))(1 - 1) - \beta_m(u(t_0))1 = -\beta_m(u(t_0)) < 0,\tag{55}$$

this is a contradiction. Hence $m(t) \leq 1$, $\forall t \in [0, T]$.

Similarly, assume now that there exists t_1 such that $m(t_1) < 0$. As $m(t)$ is continuous, that means that there exists $0 < t_0 < t_1$ such that $m(t_0) = 0$ and $m(t_0 + \epsilon) < 0$, $\forall 0 < \epsilon \leq t_1 - t_0$. However,

$$\frac{dm}{dt}(t_0) = \alpha_m(u(t_0))(1 - 0) - \beta_m(u(t_0))0 = \alpha_m(u(t_0)) > 0$$

which leads to a contradiction as well.

In conclusion $0 \leq m(t) \leq 1$, $\forall t \in [0, T]$. This property also holds for $h(t)$ and $n(t)$, respectively.

Appendix C: manufactured solution for the junction problem

A case with 3 branches having a junction at $x^{(i)} = 0$, $i = 1, \dots, 3$ is considered. The geometric parameters of the problem are $a^{(1)}(x^{(1)}) = a^{(2)}(x^{(2)}) = 2^{-2/3}a^{(3)}(x^{(3)}) = a_0$, where $x^{(i)} \in [0, L^{(i)}]$, and their lengths are given by $L^{(i)} = L$, $i = 1, 2$ and $L^{(3)} = 2^{1/3}L$. The following manufactured solutions are considered, for a

problem without current injection, that is $I(t) = 0$, $t \in [0, T]$, where $T = 10^{-5}$ s:

$$\begin{aligned}
u^{(i)}(x^{(i)}, t) &= \exp \left[-t \left(\frac{1}{C_m} \sum_{i=j}^3 g_j + \mu a_0 \left(\frac{3\pi}{2L} \right)^2 \right) \right] \sin \left(\frac{3\pi x^{(i)}}{2L} \right), \quad i = 1, 2 \\
u^{(3)}(x^{(3)}, t) &= \exp \left[-t \left(\frac{1}{C_m} \sum_{i=j}^3 g_j + \mu a_0 \left(\frac{3\pi}{2L} \right)^2 \right) \right] \sin \left(-\frac{3\pi x^{(3)}}{2^{4/3}L} \right), \\
m^{(i)}(x^{(i)}, t) &= 1, \quad i = 1, \dots, 3, \\
h^{(i)}(x^{(i)}, t) &= 1, \quad i = 1, \dots, 3, \\
n^{(i)}(x^{(i)}, t) &= 1, \quad i = 1, \dots, 3,
\end{aligned} \tag{56}$$

with $(x^{(i)}, t) \in [0, L^{(i)}] \times [0, T]$, $i = 1, \dots, 3$.

The solutions (56) satisfy the equations

$$\begin{aligned}
u_t^{(i)} &= \frac{\mu}{a^{(i)}(x^{(i)})} \left(a^{(i)}(x^{(i)})^2 u_{x^{(i)}}^{(i)} \right)_{x^{(i)}} - \frac{1}{C_m} g(m^{(i)}, h^{(i)}, n^{(i)}) u^{(i)} + f(m^{(i)}, h^{(i)}, n^{(i)}, t) + F_u \\
m_t^{(i)} &= \alpha_m(u^{(i)})(1 - m^{(i)}) - \beta_m(u^{(i)})m^{(i)} + F_m^{(i)}(u^{(i)}) \\
h_t^{(i)} &= \alpha_h(u^{(i)})(1 - h^{(i)}) - \beta_h(u^{(i)})h^{(i)} + F_h^{(i)}(u^{(i)}) \\
n_t^{(i)} &= \alpha_n(u^{(i)})(1 - n^{(i)}) - \beta_n(u^{(i)})n^{(i)} + F_n^{(i)}(u^{(i)}),
\end{aligned} \tag{57}$$

where

$$\begin{aligned}
F_u &= -\frac{1}{C_m} \sum_{j=1}^3 g_j E_j \\
F_m^{(i)}(t) &= \beta_m^{(i)}(u^{(i)}) \\
F_h^{(i)}(t) &= \beta_h^{(i)}(u^{(i)}) \\
F_n^{(i)}(t) &= \beta_n^{(i)}(u^{(i)})
\end{aligned} \tag{58}$$

and the boundary conditions are

$$\begin{aligned}
u^{(i)}(0, t) &= 0, \\
\sum_{i=1}^3 \left(a^{(i)} \right)^2 u_{x^{(i)}}^{(i)}(0) &= 0, \\
u_{x^{(i)}}^{(i)}(L^{(i)}) &= 0, \quad i = 1, 2, \\
u^{(3)}(x^{(3)}, t) &= \exp \left[-t \left(\frac{1}{C_m} \sum_{i=j}^3 g_j + \mu a_0 \left(\frac{3\pi}{2L} \right)^2 \right) \right].
\end{aligned} \tag{59}$$

The numerical values chosen for each physical constant are the same as the ones reported in Table 1 and 2.

Appendix D: manufactured solution for the cable with soma problem

A problem with constant cable radius $a(x) = a_0$, $x \in [0, L]$ and without current injection, that is $I(t) = 0$, $t \in [0, T]$, where $T = 10^{-5}$ s:

$$\begin{aligned} u(x, t) &= \exp \left[-t \left(\frac{1}{C_m} \sum_{j=1}^3 g_j + \mu a_0 \left(\frac{\beta}{L} \right)^2 \right) \right] \cos \left(\frac{\beta x}{L} \right) \\ m(x, t) &= 1 \\ h(x, t) &= 1 \\ n(x, t) &= 1 \end{aligned} \tag{60}$$

where $(x, t) \in [0, L] \times [0, T]$ and β satisfies $\frac{\tan \beta}{\beta} = -\frac{\mu}{\eta a_0 L}$.

The solutions (60) satisfy the equations

$$\begin{aligned} u_t &= \frac{\mu}{a(x)} (a(x)^2 u_x)_x - \frac{1}{C_m} g(m, h, n) u + f(m, h, n, x, t) + F_u(t) \\ m_t &= \alpha_m(u)(1 - m) - \beta_m(u)m + F_m(u) \\ h_t &= \alpha_h(u)(1 - h) - \beta_h(u)h + F_h(u) \\ n_t &= \alpha_n(u)(1 - n) - \beta_n(u)n + F_n(u) \end{aligned} \tag{61}$$

where

$$\begin{aligned} F_u(t) &= -\frac{1}{C_m} \sum_{j=1}^3 g_j E_j \\ F_m(t) &= \beta_m(u) \\ F_h(t) &= \beta_h(u) \\ F_n(t) &= \beta_n(u) \end{aligned} \tag{62}$$

and the boundary conditions

$$\begin{aligned} u_x(0) &= 0 \\ u_t(L) &= -\eta a(L)^2 u_x(L) - \frac{1}{C_m} g(m(L), h(L), n(L)) + f(m(L), h(L), n(L), L, t) + F_b(t) \end{aligned} \tag{63}$$

where

$$F_b(t) = -\frac{1}{C_m} \sum_{j=1}^3 g_j E_j. \tag{64}$$

The numerical values chosen for each physical constant are provided in Tables 1 and 5.

References

- [1] A. Hodgkin, A. Huxley, A quantitative description of membrane current and its application to conduction and excitation in nerve, *Journal of Physiology* 117 (1952) 500–544.
- [2] W. Rall, Membrane potential transients and membrane time constant of motoneurons, *Experimental Neurology* 2 (1960) 503–532.
- [3] M. Hines, Efficient computation of branched nerve equations, *International journal of bio-medical computing* 15 (1984) 69–76.

- [4] A. Kellems, S. Chaturantabut, D. Sorensen, S. Cox, Morphologically accurate reduced order modeling of spiking neurons, *Journal of computational neuroscience* (2010) 1–18.
- [5] D. Amsallem, J. Roychowdhury, ModSpec: An open, flexible specification framework for multi-domain device modelling, *IEEE/ACM Conference on Computer-Aided Design* (2011).
- [6] M. Mascagni, The backward Euler method for numerical solution of the Hodgkin-Huxley equations of nerve conduction, *SIAM Journal on Numerical Analysis* 27 (1990) 941–962.
- [7] M. Hanslien, K. H. Karlsen, A. Tveito, A Maximum Principle for an Explicit Finite Difference Scheme Approximating the Hodgkin-Huxley Model, *BIT Numerical Mathematics* 45 (2005) 725–741.
- [8] M. Carpenter, J. Nordström, D. Gottlieb, A stable and conservative interface treatment of arbitrary spatial accuracy, *Journal of Computational Physics* 148 (1999) 341–365.
- [9] J. Nordström, M. Carpenter, Boundary and interface conditions for high-order finite-difference methods applied to the Euler and Navier–Stokes equations, *Journal of Computational Physics* 148 (1999) 621–645.
- [10] J. Nordström, M. H. Carpenter, High-order finite difference methods, multidimensional linear problems, and curvilinear coordinates, *Journal of Computational Physics* 173 (2001) 149–174.
- [11] K. Mattsson, M. Svärd, J. Nordström, Stable and accurate artificial dissipation, *Journal of Scientific Computing* 21 (2004) 57–79.
- [12] K. Mattsson, J. Nordström, Summation by parts operators for finite difference approximations of second derivatives, *Journal of Computational Physics* 199 (2004) 503–540.
- [13] M. Svärd, M. H. Carpenter, J. Nordström, A stable high-order finite difference scheme for the compressible Navier–Stokes equations, far-field boundary conditions, *Journal of Computational Physics* 225 (2007) 1020–1038.
- [14] M. Svärd, J. Nordström, A stable high-order finite difference scheme for the compressible Navier–Stokes equations, *Journal of Computational Physics* 227 (2008) 4805–4824.
- [15] J. Nordström, J. Gong, E. van der Weide, M. Svärd, A stable and conservative high order multi-block method for the compressible Navier–Stokes equations, *Journal of Computational Physics* 228 (2009) 9020–9035.
- [16] J. Lindström, J. Nordström, A stable and high-order accurate conjugate heat transfer problem, *Journal of Computational Physics* 229 (2010) 5440–5456.
- [17] J. Berg, J. Nordström, Stable Robin solid wall boundary conditions for the Navier-Stokes equations, *Journal of Computational Physics* 230 (2011) 7519–7532.
- [18] J. Gong, J. Nordström, Interface procedures for finite difference approximations of the advection–diffusion equation, *Journal of Computational and Applied Mathematics* 236 (2011) 602–620.
- [19] J. P. Keener, J. Sneyd, *Mathematical Physiology, Cellular Physiology*, Springer Verlag, second edition edition, 2009.
- [20] B. Gustafsson, H.-O. Kreiss, J. Oliger, *Time Dependent Problems and Difference Methods*, Wiley-Interscience, 1995.
- [21] K. Mattsson, Summation by parts operators for finite difference approximations of second-derivatives with variable coefficients, *Journal of Scientific Computing* 51 (2012) 650–682.

- [22] J. Nordström, M. Svard, Well-posed boundary conditions for the Navier-Stokes equations, *SIAM Journal on Numerical Analysis* (2005) 1231–1255.
- [23] P. M. Knupp, K. Salari, *Verification of computer codes in computational science and engineering*, CRC Press, 2003.
- [24] U. Bhalla, D. Bilitch, J. Bower, Rallpacks: a set of benchmarks for neuronal simulators, *Trends in neurosciences* 15 (1992) 453–458.
- [25] C. Koch, *Biophysics Of Computation, Information Processing In Single Neurons*, Oxford University Press, USA, 2004.